J. Fluid Mech. (1988), *vol.* 193, *pp.* 171–189
Printed in Great Britain

Unsteady attached cavitation on an oscillating hydrofoil

By J. P. FRANC AND J. M. MICHEL
Institut de Mécanique de Grenoble, Université de Grenoble, B.P. 68 – 38402, Saint-Martin-d'Hères Cédex, France

(Received 9 July 1987 and in revised form 26 November 1987)

A series of visualizations of non-cavitating and cavitating unsteady flows around an oscillating hydrofoil has been carried out in order to investigate the effect of unsteadiness on attached cavitation. The major conclusion of the present experimental analysis is that the strong interaction that was previously pointed out in the case of steady cavitation between an attached cavity and the boundary layer which develops upstream cavity detachment, still plays a prominent role in unsteady cavitation. We propose to generalize for the case of unsteady attached cavitation the two following points which were initially established under steady conditions and which constitute a cavitation detachment criterion:

(i) a cavity detaches behind laminar separation of the boundary layer;

(ii) transition to turbulence sweeps away an attached cavity.

1. Introduction

In a previous paper (Franc & Michel 1985), the authors studied the connection between the boundary layer which spreads out on a smoothly curved wall – namely, one circular and two elliptical cylinders, plus one symmetrical NACA 16012 hydrofoil – and a largely developed cavity which starts from this wall. After other authors (Alexander 1968; Arakeri & Acosta 1973; Van der Meulen 1980) who centred their studies on incipient cavitation, they found that the detachment point of an attached cavity is strongly connected to the laminar separation of the boundary layer. It was also established, as a counterpart, that natural transition to turbulence inside the boundary layer prevents the existence of an attached cavity, in all experimental cases under examination, which covered a large enough range in Reynolds number, cavitation number and angle of attack, and thus in pressure gradient.

The details of the local mechanisms which create the link between the cavity detachment and the laminar separation are not known. At most we can say that the cavity detachment needs a zone of still flow ahead of it and that the turbulent velocity and pressure fluctuations are not likely to be compatible, either by their timescale or by their amplitude scale, with a free surface which, hypothetically, would detach downstream of a turbulent separation. However, the global effect of that link is considerable and, by some aspects, unexpected. For instance, the laminar separation requires an adverse pressure gradient so that the cavity detaches downstream of the minimum pressure point: the liquid particles sustain negative pressures without any vaporization, this being possible if the liquid is poor in gas nuclei which otherwise would react as weak spots for the continuum medium. Now if a developed cavity is established at the rear part of a hydrofoil, a slight increase

in the external turbulence can be sufficient to trigger the boundary-layer transition, which sweeps the cavity away. The flow returns to the non-cavitating regime and the negative pressures work for a longer time on the liquid particles. In this case, the turbulent flow increases the extent of the thermal non-equilibrium state of the liquid.

In the present study, the flow is made unsteady by the periodic oscillation in incidence of the NACA 16012 hydrofoil. That constrained configuration was used by a number of investigators in the field of aerodynamics, but in hydrodynamics of cavitating flows the experimental and theoretical studies are only few. Shen & Peterson (1978, 1980) investigated cavitation inception and leading-edge sheet cavitation on an oscillating two-dimensional hydrofoil. They showed that cavitation inception is significantly delayed by the oscillation. They also developed a simplified model based on Giesing's method (Giesing 1968) of unsteady potential flow calculation for predicting the cavitation inception in the case of small pitching amplitude. Shen & Gowing (1986) measured the pressure fluctuations and found that the potential theory agrees with the experiments in the case of the non-cavitating flow and for the small values of the reduced frequency, but it becomes inadequate as soon as dynamic stall appears. In the cavitating regime, the pressure response at the wall is strongly affected by the passage of the cavity termination. Bark & Van Berlekom (1978), Kruppa & Sasse (1982) were concerned with the effect of unsteadiness on noise and erosion produced by the cavitating flows. In those experiments, the global response of the flow to the periodic excitation was found to be periodic. This is true also in our case, even for the flows with largely developed cavities.

From a practical viewpoint, the use of an oscillating hydrofoil is intended to give useful information in fields of application where unsteadiness plays an appreciable role. An example is found in marine propellers, in which unsteady cavitation results from the varying pressure and velocity conditions encountered by each propeller blade over one revolution. Of particular importance for the designer is the question: is the so-called 'quasi-steady modelling' relevant to the description of the flow around the propeller? In other words, is it possible to neglect the time-dependence of the inertial forces and its associated delays? Even if its implications are restricted to the case of the two-dimensional laboratory flow, the question involves several intricate aspects, which touch on the modelling itself and the experimentation, as we learn from unsteady aerodynamics, to which cavitation brings its own complexity.

Here we take the problem from a rather simple point of view and we adopt the method which proved to be successful in the former study, in which largely cavitating flows are compared with non-cavitating flows by means of visualization techniques. The use of dye injection and the taking of fast films allows us to follow the main characteristic points on the hydrofoil upper side and to build space–time diagrams which make visible the phenomenon evolution. Thus, within the limits of the experimental conditions, one can consider the main underlying questions of the study: what happens to the boundary layer–cavity detachment connection when it is submitted to a forced motion? Can this motion eliminate the attached cavity, as is done by the turbulent fluctuations of the boundary layer in the steady case? How do the delay-times vary with the excitation frequency and the development of cavitation? In addition, some global force measurements will show that, despite formal resemblances, non-cavitating and cavitating flows behave differently because of the two-phase nature of the latter.

The experimental set-up and the experimental conditions are described in §2. Note that, in view of the phenomena to be observed, the hydrodynamic tunnel which is used has to fulfil two chief requirements: firstly water must be strongly deaerated and secondly the test section must be uncoupled from the other parts of the loop. In §3, the main experimental data are given. In §4 and 5, we study the global unsteady effects and we examine the detachment criterion which was established previously in the steady case. Then we had numerical models – potential flow and boundary-layer integral method – at our disposal so that it was possible to attain the effective prediction of the detachment location for slender hydrofoils. Those computations helped to strengthen the conclusions of the experimental investigation. In the unsteady case, boundary-layer computations are available but, to the authors' knowledge, no efficient numerical model for the potential cavity flow exists: the positions of the detachment points on both the upper and lower sides are two unknown functions of time, which brings an important practical complexity to the computation. In addition, the way by which the rear part of the cavity must be modelled is not clear, if one considers either the pressure condition at infinity (Woods 1964; Benjamin 1964) or the flow reattachment to the solid wall in the case of partial cavitation. Thus a detachment criterion does not lead to practical predictions in the present state of the numerical techniques but is has to be taken purely as a physical conclusion.

2. Experimental set-up and experimental conditions

The tests were carried out in the second free-surface channel of the hydrodynamic tunnel at Grenoble University. The test section is 1.6 m long, 0.12 m wide and 0.40 m high. The frec-stream velocity U is in the range 2.5–13 m/s; thus, the Reynolds number $Re = \rho Uc/\mu$ based on the foil chord c, $c = 0.10$ m, is in the range 0.25×10^6–1.3×10^6. The cavitation index $\sigma_v = (p_0 + \rho gh - p_v)/\frac{1}{2}\rho U^2$, where g is the gravity acceleration, $h = 0.20$ m the submersion depth of the body, p_0 the absolute pressure at the free surface, and p_v the vapour pressure, can be reduced to 0.03. The free-stream turbulence intensity varies from 0.12 to 0.16% when the velocity U varies from 3 to 12 m/s. Without nuclei injection, which constitutes the practical operating condition in the present investigation, the average nuclei density is very small (between 0.05 and 0.3 per cm^3); such a very low nuclei content of the water accounts for a sheet cavitation and no travelling bubble cavitation. The foil is made with stainless steel and its surface roughness is about 0.1 μm.

The hydrodynamic tunnel, on which the experiments described here have been carried out, is particularly favourable to the experimental study of unsteady flows. The presence of a free surface together with the existence of large upstream and downstream tanks (Rowe & Kueny 1980) ensures a complete hydraulic decoupling between the test section and the remainder of the circuit. Therefore, upstream flow conditions are insensitive to the foil oscillations and can be well controlled.

The oscillation mechanism is shown schematically in figure 1. It produces an oscillation of the foil around mid-chord at a dimensional frequency f up to 25 Hz which corresponds to a reduced frequency $f^* = fc/U$ up to 1. The so-defined reduced frequency f^* measures the ratio between the time of convection along the chord length c at the free-stream velocity U and the duration of the oscillation period. The maximum oscillation amplitude $\Delta\alpha$ can vary up to $+5°$ and the mean angle of attack can be adjusted between $-10°$ and $+10°$. The oscillation is approximately

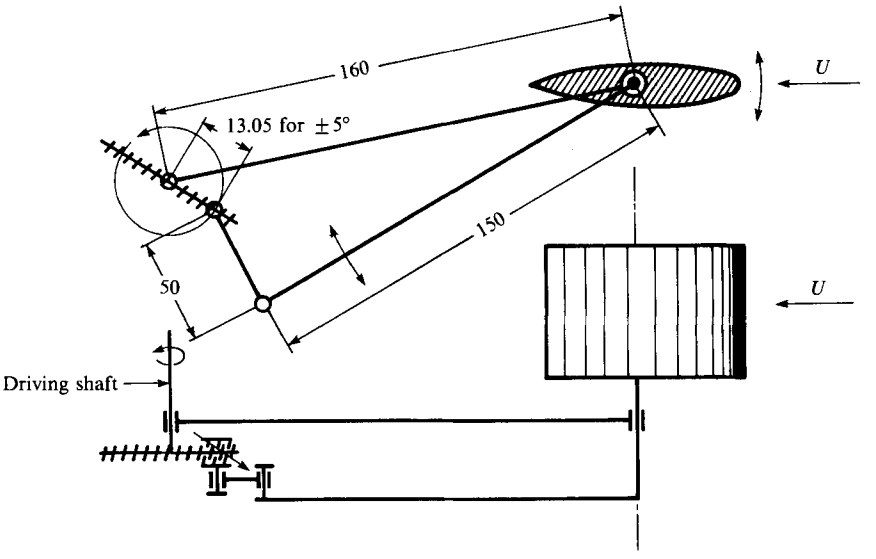

FIGURE 1. Principle of the oscillation mechanism. (The mean angle of attack is adjusted by a general rotation of the mechanism.)

sinusoidal: the first and second harmonics represent only 6% and 2‰ of the fundamental. The force coefficients – lift, drag and moment – are measured through a dynamometric bar whose lowest natural frequency is 120 Hz.

The boundary layer is visualized by dye injection at the leading edge through a hole of 0.2 mm in diameter; this simple technique has proved to be as efficient for unsteady flow as it was for steady flow. It allows us to locate the characteristic points of the boundary layer with sufficient precision for the global analysis we have in view. A turbulent zone is characterized by a much higher degree of diffusion of dye than a laminar zone. Therefore we can distinguish points of transition from laminar to turbulent and inversely. Note that the term 'transition' has to be used here with care. For instance, in the case of 'transition' from laminar to turbulent, the point of transition simply refers to the locus of discrimination of an upstream laminar zone from a downstream turbulent zone at a given time in the period. To know if there is, strictly speaking, transition of laminar fluid particles to turbulence as they move downstream we have to compare the celerity of the 'transition' point to the speed of particles; if the celerity of the transition point is strictly lower than the speed of particles, laminar particles actually undergo transition to turbulence as they pass beyond the transition point; if the celerity of the transition point equals the local speed of fluid particles, there is no actual transition. In a similar way, the term transition turbulent/laminar is used to characterize the locus of discrimination of an upstream turbulent zone from a downstream laminar zone at a given time in the period. The dye-injection technique also allows us to distinguish separated zones from non-separated zones at any given time in the period. Separated zones correspond to points of the foil where the dye, which visualizes a fluid line, does not cling close to the wall. Such zones are limited by two special points which are called later, separation and reattachment. The same type of difficulty arises concerning these terms; they do not prevail on the fluid particles actually to separate from the foil or to reattach to the foil; they simply characterize a snapshot of the flow.

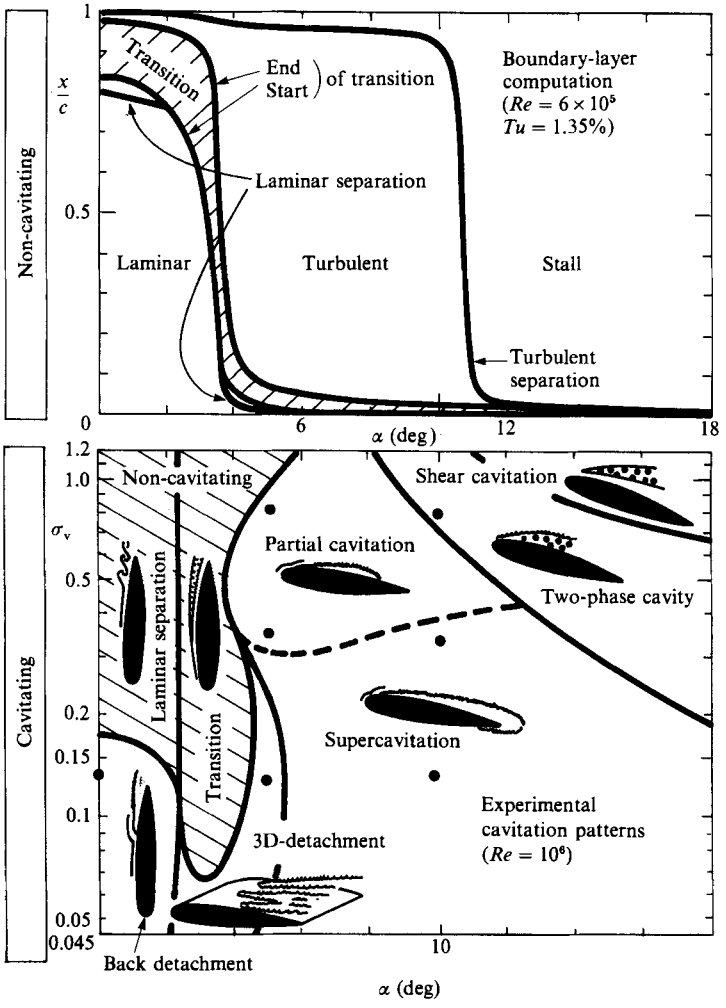

FIGURE 2. Boundary-layer state and cavitation patterns for steady non-cavitating and cavitating flows around the NACA 16-012 hydrofoil. (Points indicate the main test conditions for the oscillating hydrofoil.)

The results presented here are directly issued from simple observation of the unsteady cavity and simultaneous visualization of the unsteady boundary-layer flow. They are supported by the analysis of about fifty high-speed films at a framing rate up to 5500 pictures per second. As a reference, we recall in figure 2 results previously obtained concerning the boundary-layer state and cavitation patterns for steady non-cavitating and cavitating flows around the NACA 16-012 hydrofoil. Note that the frontiers between the different cavitation patterns presented in figure 2 have been determined by increasing angles of attack for a constant value of the cavitation parameter σ_v and that some hysteresis may occur for decreasing angles of attack. Such an effect is presented on figure 3 which presents the cycle that the lift coefficient describes versus the angle of attack during quasi-steady oscillations under cavitating and non-cavitating conditions. For instance, in the cavitating case ($\sigma_v = 0.13$), when the angle of attack increases, the leading-edge cavity appears at about 8° and involves a decrease in lift. When the angle of attack decreases, the cavity does not

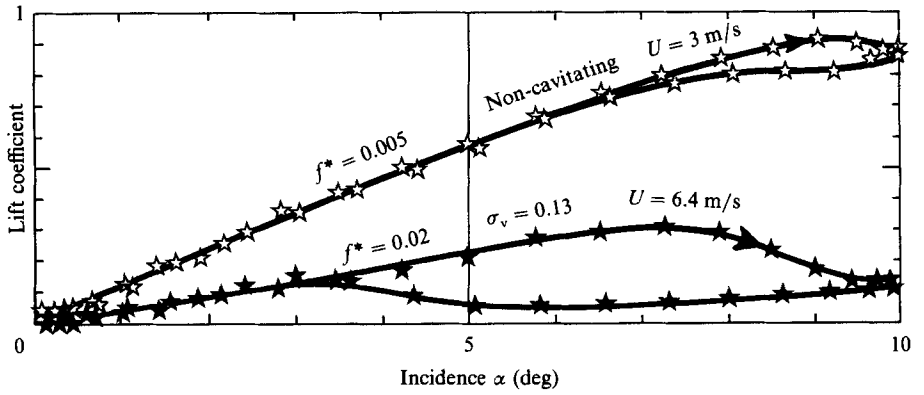

FIGURE 3. Lift coefficient versus incidence under quasi-steady oscillation for $\bar{\alpha} = 5°$ and $\Delta\alpha = \pm 5°$.

vanish for the same value of the angle of attack but for a lower value of about 4°; then, the lift finds again its non-cavitating value as for increasing angles of attack. Another point in figure 2 deserves consideration. It appears that cavities detach from the leading edge in the range of incidence 4–6° to 11° for which, in the non-cavitating regime, the flow is turbulent over the foil upper side. That is possible because a small laminar separated bubble currently appears in front of the turbulent region. Moreover, in some circumstances, it happens that the pressure distribution is modified by the cavity itself so that a new laminar separation occurs at the place where before a turbulent flow was established.

Visualizations and films have been performed principally for three characteristic values of the mean angle of attack $\bar{\alpha} = 0°$, 5° and 10°. The oscillation amplitude was generally fixed at its maximum value +5°. This ensures that the flow goes through different cavitating regimes during oscillation, as can be seen on figure 2, and thus leads to the most interesting cases. For example, in the case $\sigma_v = 0.13$, $\bar{\alpha} = 0°$, the foil goes across three different domains, which actually appear for the lower values of f^*, i.e. in quasi-steady conditions. Four different values of the cavitation parameter which cover a large enough variety of cavitation expansion have been tested: $\sigma_v = 0.13$, 0.33, 0.81 and non-cavitating. For each case, the oscillation frequency varies up to 21 Hz. Under non-cavitating conditions, tests were carried out at the minimum speed of 3 m/s in order to get a reduced frequency as high as possible; under cavitating conditions a middle value of the speed of 6 m/s was generally chosen, which decreases the maximum reduced frequency but conversely allows sufficiently low values of the cavitation parameter to be obtained. The change in Reynolds number which resulted from that choice is of minor importance as we know from experience. All the results presented here are relative to the upper-side of the NACA 16-012 hydrofoil.

In order to evaluate the range of the present flow unsteadiness, some estimations are made concerning the characteristic times and the velocity fluctuations. The forced motion period $1/f$ is 0.04 s at its minimum, while the convection time c/U is in the interval 0.01–0.04 s. This last quantity is also an approximate measure of the time which is needed for the establishment of the boundary layer under an impulsive motion from rest (Schlichting 1959). Similarly, for a cavitating flow where cavity length l is larger than c, the response time to a sudden variation of one of the control parameters is l/U. Here the mean value of the ratio l/c is approximately between 0.1

and 5, and its instantaneous values can vary from 0 to 10. Thus the global motion gives various experimental conditions. Reference values can also be looked for in the direction of the turbulent boundary layer. On one side the maximum relative turbulent fluctuation u'/U is between 5 and 10%, while its duration is of the order of δ/u', where δ is the boundary layer thickness. This value does not give more than 0.001 s. On the other side, it appears from a potential flow calculation of the unsteady non-cavitating flow (Franc 1986) which is based on the method developed by Basu & Hancock (1978), that in the case $\bar{\alpha} = 0°$, $\Delta\alpha = 5°$, $f^* = 0.2$, the velocity with respect to the foil undergoes fluctuations which are of the order 7%. This is obtained at the abscissa $x = 0.94c$, which can be considered significant for the phenomena we have in view, whereas the velocity fluctuations in the leading-edge vicinity are one order of magnitude larger. Thus the forced motion produces fluctuation amplitudes comparable with turbulent fluctuations but its basic timescale is clearly larger than the turbulent characteristic time. As a conclusion, the temporal derivatives in the present experiments are sufficient to produce large global values, but they do no reach the characteristic values of the boundary-layer turbulence.

3. Main experimental data

The structure of cavitating and non-cavitating unsteady flows can be summarized on space–time diagrams which proved to be a convenient representation for further discussion. Each diagram constitutes a primary digest of a complete film. It characterizes a typical period and is free of secondary three-dimensional effects (as cavitation on channel walls) which could make direct interpretation of some films difficult to an inexperienced observer. This is why we prefer to give space–time diagrams, although a few extracts from films are presented. On such diagrams, the reduced abscissa x/c of the characteristic points of the cavity (as detachment or closure) and of the boundary layer flow (as transition or separation) are plotted at every reduced time ft in the period. At time $t = 0$, the foil is supposed to go up through its mean position. These abscissae are directly deduced from the analysis of the high-speed films. Space–time diagrams are divided into different complementary domains (as laminar/turbulent domains or non-separated/separated domains); such a representation enables us to find the structure of the unsteady non-cavitating and cavitating flows at any point of the foil and at any time in the period for a given oscillatory movement and for given free-stream velocity and pressure values.

3.1. *Small mean angle of attack* ($\bar{\alpha} = 0°$)

As an example, figure 4(*a*) is discussed below. It corresponds to oscillations of amplitude $\Delta\alpha = \pm 5°$ around a mean angle of attack $\bar{\alpha} = 0°$ at a reduced frequency $f^* = 0.25$ under non-cavitating conditions. The following steps are observed.

(i) There is a given time in the period ($ft \approx 0.4$) at which turbulence bursts out in a given point of the foil $x/c \approx 0.3$;

(ii) from this time, this point divides into two fronts which move apart, an upstream front and a downstream front which limit the turbulent zone;

(iii) the upstream front first moves a bit upstream; this means that there is contamination of laminar zones by turbulence. Then it moves downstream, with a speed slightly lower than free-stream velocity; so, a few laminar fluid particles turn to turbulence as they move downstream;

(iv) before turbulence appears, the laminar boundary layer separates at $x/c \approx 0.8$;

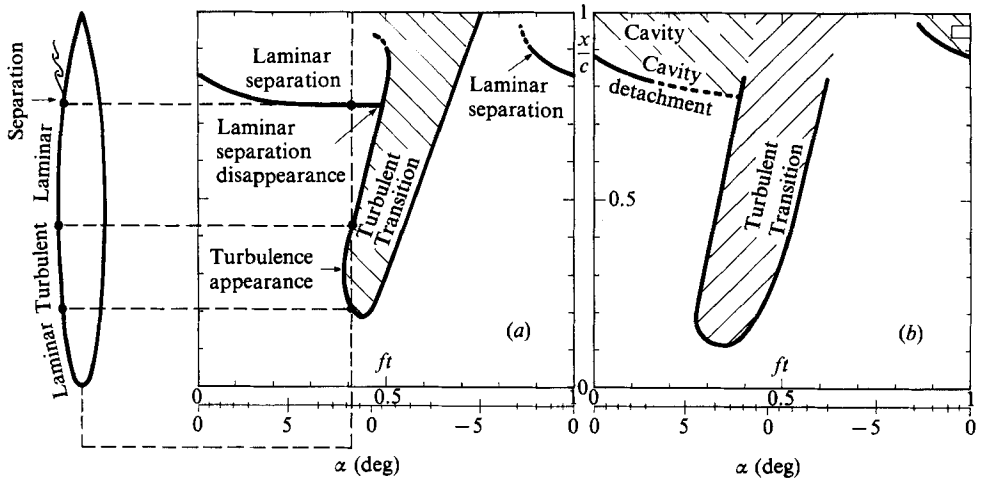

FIGURE 4. Space–time diagrams for $\bar{\alpha} = 0$ and $\Delta\alpha = \pm 5°$. (*a*) Non-cavitating: $f^* = 0.25$; $U = 3$ m/s; $Re = 3 \times 10^5$. (*b*) Cavitating: $f^* = 0.22$; $\sigma_v = 0.13$; $U = 6.9$ m/s; $Re = 6.9 \times 10^5$.

(v) laminar separation still exists when turbulence appears; it vanishes only when it is reached by the downstream turbulent front which is simply convected at the free-stream velocity (cf. §4);

(vi) when the upstream turbulent front reaches the trailing edge, the boundary-layer flow is again fully laminar and a laminar separation reappears at the rear of the foil. It appears near the trailing edge and then moves rapidly upstream up to its average position $x/c \approx 0.8$. Between turbulence disappearance and laminar separation reappearance, the flow visualization at the back of the foil is poor, and the interpretation of the boundary-layer flow is difficult during this period of time.

Under cavitating conditions, other things being equal, the main difference, apart from minor quantitative variations, is that the separated domain behind laminar separation is filled with a vapour cavity as shown in figure 4(*b*). Cavitation detachment behaves quite like laminar separation. In particular the cavity vanishes as soon as cavity detachment is reached by the turbulent front; it reappears when the boundary layer has again become fully laminar and detaches initially near the trailing edge before moving a bit upstream, as is the case for laminar separation under non-cavitating conditions.

3.2. *Medium mean angle of attack* ($\bar{\alpha} = 5°$)

For the medium value of the mean angle of attack $\bar{\alpha} = 5°$, considering the oscillation amplitude $\Delta\alpha = \pm 5°$, the oscillation goes through the static stall angle of about 9°. Therefore, under non-cavitating conditions a separated domain is observed inside the turbulent domain as shown on figure 5(*a*). The scenario of development of the separated zone, which is characteristic of dynamic stall, is presented below.

(i) At a given time in the period which depends upon reduced frequency, the flow is inclined to separate from the foil at a given point of the turbulent region, in the neighbourhood of the leading edge;

(ii) at an early stage, this separated zone is small: its upstream front (separation point) and its downstream front (reattachment point) are very close; in addition, its height is initially small;

(iii) as soon as turbulent separation has appeared, both fronts move aside in a way

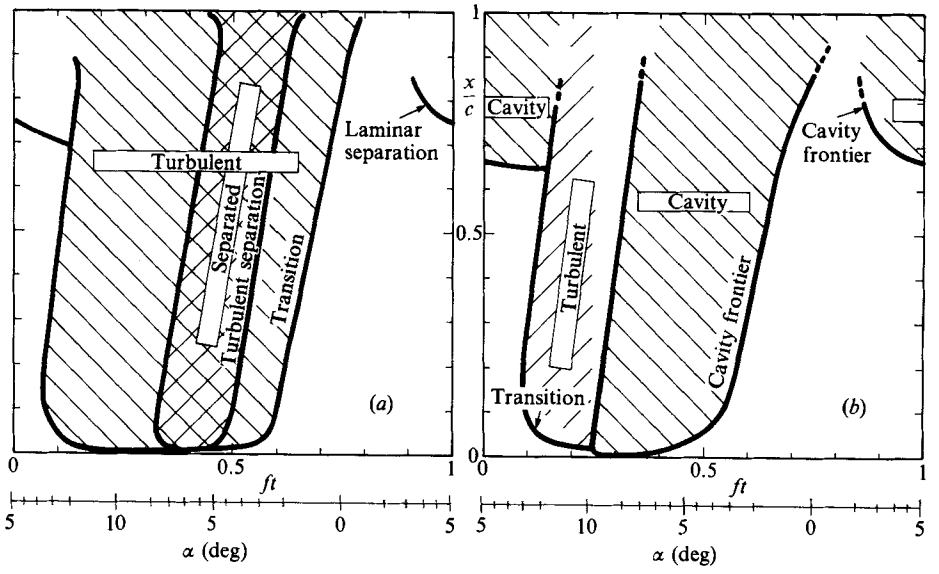

FIGURE 5. Space–time diagrams for $\bar{\alpha} = 5°$ and $\Delta\alpha = \pm 5°$. (*a*) Non-cavitating: $f^* = 0.15$; $U = 3$ m/s; $Re = 3 \times 10^5$. (*b*) Cavitating: $f^* = 0.14$; $\sigma_v = 0.13$; $U = 6.3$ m/s; $Re = 6.3 \times 10^5$.

similar to the upstream and downstream fronts of the turbulent zone already described. The reattachment point moves downstream at about the free-stream velocity U. The separation point moves a bit upstream, stays in the vicinity of the leading edge and then moves downstream at about the velocity U; when it reaches the trailing edge, the turbulent boundary-layer flow is again fully attached to the foil.

The development of cavitation brings little change from a qualitative viewpoint to the non-cavitating flow scheme which has been presented, as shown on figure 5(*b*). Two different cases occur:

(i) if cavitation is very much developed (low values of the cavitation parameter), both separated zones – behind laminar separation at the back of the foil and at leading edge – are filled with a cavity;

(ii) if cavitation is little developed, only the separated zone at the leading edge is filled with a cavity.

Figure 5(*b*) illustrates the former case.

3.3. *Large mean angle of attack* ($\bar{\alpha} = 10°$)

In the case of a large mean angle of attack, under non-cavitating conditions the boundary layer is turbulent nearly from the leading edge during the whole cycle.

As in the previous case, a separated zone from the leading edge is observed during part of the cycle (figure 6*a*). Under cavitating conditions, it is filled with a cavity which detaches from the leading edge as shown on figure 6(*b*) and which is characteristic of cavitating dynamic stall.

Note that dynamic stall was found to develop only in the vicinity of leading edge. That may be connected to the position of the rotation axis, which is in the midst of the chord and not at the quarter-point, contrary to most of the other experimental works.

Visualizations of dynamic stall are presented in figure 7. Two consecutive periods in the same film are shown corresponding to the same conditions of the flow and

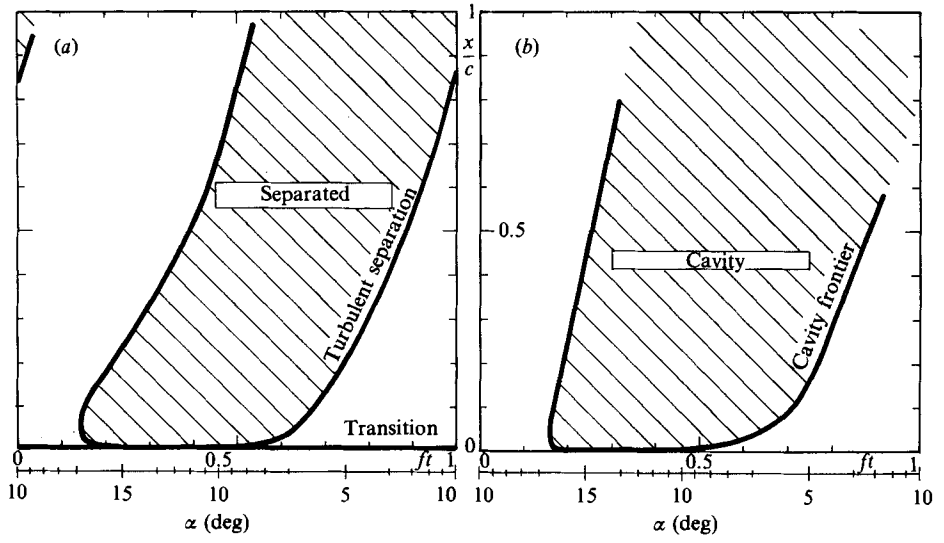

FIGURE 6. Space–time diagrams for $\bar{\alpha} = 10°$ and $\Delta\alpha = \pm 5°$. (*a*) Non-cavitating: $f^* = 0.25$; $U = 3$ m/s; $Re = 3 \times 10^5$. (*b*) cavitating: $f^* = 0.25$; $\sigma_v = 0.33$; $U = 6$ m/s; $Re = 6 \times 10^5$.

oscillation. The first one is non-cavitating whereas the second one is cavitating. This is due to the high value of the cavitation parameter ($\sigma_v = 1.77$) which sets the flow at the limit between cavitating flow and non-cavitating flow so that the least disturbance makes cavitation explode. Incidentally, it shows that the size of vapour structures may not gradually grow from zero as the cavitation parameter is gradually lowered; actually, incipient cavitation may be developed already. The leading-edge cavitating structure generally appears from three-dimensional sources of cavitation as the central injection hole (time $t/T = 1.26$) or the boundary layers on the tunnel wall ($t/T = 2.29$). However, the flow is two-dimensional during most of the period. We clearly see on images 13 to 18 (times 1.26–1.69), that the flow rolls up at cavity termination. The so-formed re-entrant jet breaks the free surface of the cavity (images 17–18) and gives birth in the present case to two vapour substructures (images 19–21) which collapse (images 19–20), rebound (image 21, $t/T = 2.03$) and collapse again (image 25, $t/T = 2.29$) when a new cavitating vortex structure is formed at the leading edge.

4. Main unsteady effects

Visualizations of unsteady non-cavitating and cavitating flows around the oscillating hydrofoil have shown that phenomena which appear at the head of the foil move along the foil towards the trailing edge with time. It is the case of upstream and downstream fronts of turbulence, separation and reattachment of the turbulent boundary-layer flow, detachment and closure of the leading-edge cavity. On the other hand, laminar separation and cavity detachment when they appear at the rear of the foil for low angles of attack do not undergo such a regular backward motion and only move in a limited region for a limited time in the neighbourhood of the trailing edge as mentioned in §3.1 (see figures 4 and 5).

This backward motion is recognizable on space–time diagrams (see for instance figures 4–6) as the location of the above-mentioned characteristic points is principally

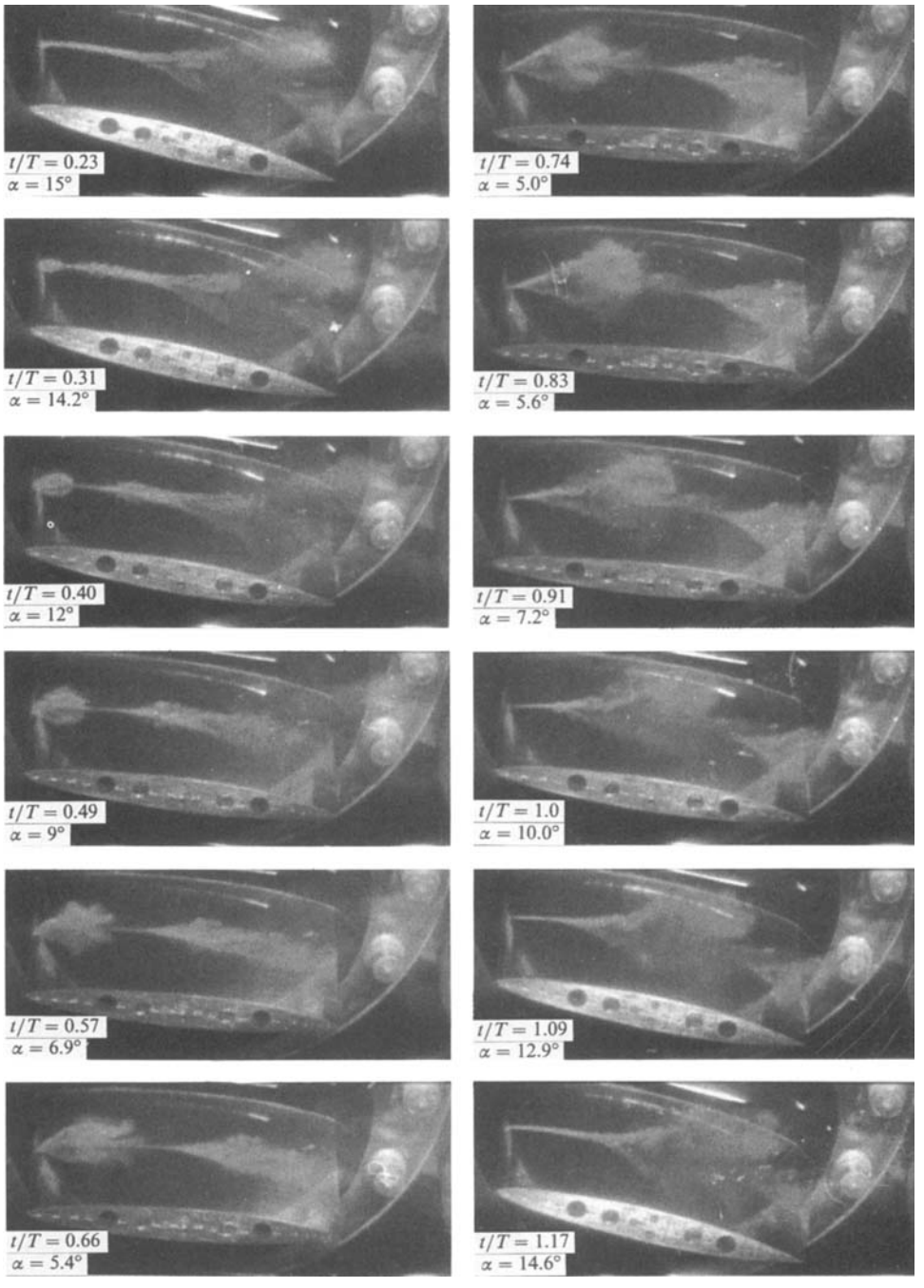

FIGURE 7. For caption see page 183.

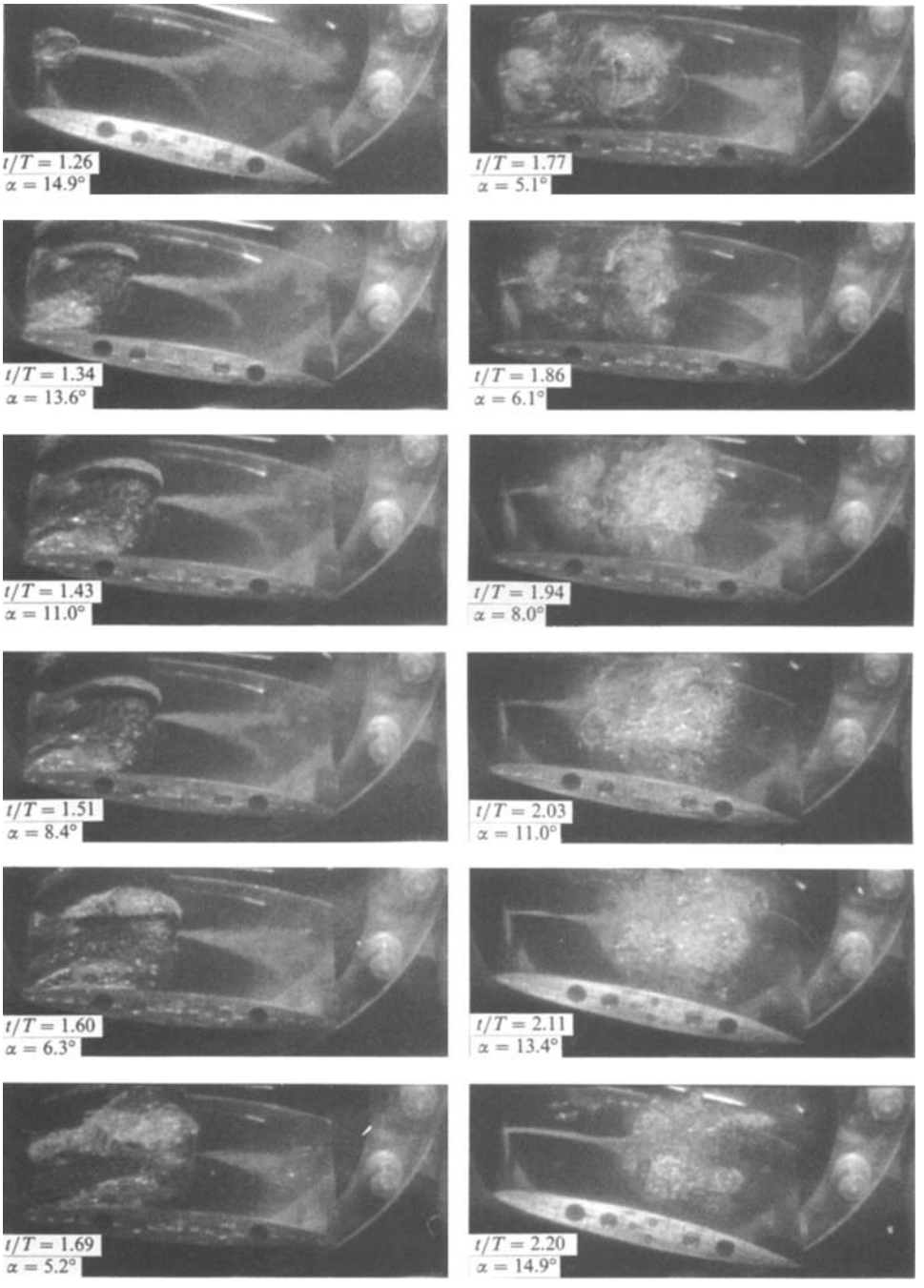

FIGURE 7. For caption see facing page.

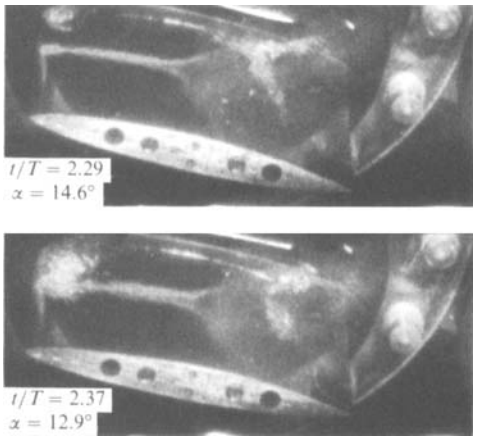

FIGURE 7. Visualizations of non-cavitating and cavitating dynamic stall for $\bar{\alpha} = 10°$; $\Delta\alpha = \pm 5°$; $\sigma_v = 1.77$; $U = 3.1$ m/s; $f = 21$ Hz; $f^* = 6.08$; $T = 47.6$ ms. (Time between two consecutive images: 4.08 ms.)

made of a straight line whose slope decreases when the reduced frequency increases. The estimation of the slope gives directly the order of magnitude of the velocity. In reduced coordinates $(x/c, ft)$, it is of the order of $1/f^*$; this means that the corresponding phenomena are simply convected downstream with the free-stream velocity. Convection is the first main unsteady effect which was pointed out by visualizations.

As an example of the convection effect, the shedding of a vortical structure associated with dynamic stall which is presented in figure 7 can be analysed as follows. Visualizations have proved that turbulent separation keeps attached to the leading edge during a fraction β of the oscillation period T. During this period of time, turbulent reattachment is convected downstream approximately with the free-stream velocity U. The size of the corresponding separated structure, i.e. the distance between separation and reattachment, increases up to βUT after time βT (see figure 8). From that time, separation, in turn, is convected downstream with velocity U. So, the structure breaks away from the leading edge and is convected on the foil with velocity U keeping approximately the same size βUT. Therefore, dynamic stall produces a well-defined structure only if its size βUT is sufficiently low compared with the foil size c. This implies that the reduced frequency f^* has to be sufficiently high, say greater than β. It is tantamount to supposing that its lifetime c/U is sufficiently greater than its growth time βT. In the case $\bar{\alpha} = 10°$, $\Delta\alpha = 5°$ and in the domain of reduced frequency presently investigated, the fraction β is of the order of $\frac{1}{2}$, i.e. it takes approximately half a period for the structure to grow up to its final size. So the threshold frequency above which the size of the structure is lower than the size of the foil is about 0.5.

This upper-side structure is a clockwise vortex. This is due to the fact that separation and reattachment are locally points of flow reversal as the visualization shows. The reversed flow which develops between these two points, associated with the external free stream creates a shear which tends to roll-up the structure clockwise. Under cavitating conditions, the core of this structure which is a low-pressure zone due to rotation, is filled with vapour as shown on figure 7.

The second unsteady effect which comes out from visualization is delay. Figure 9

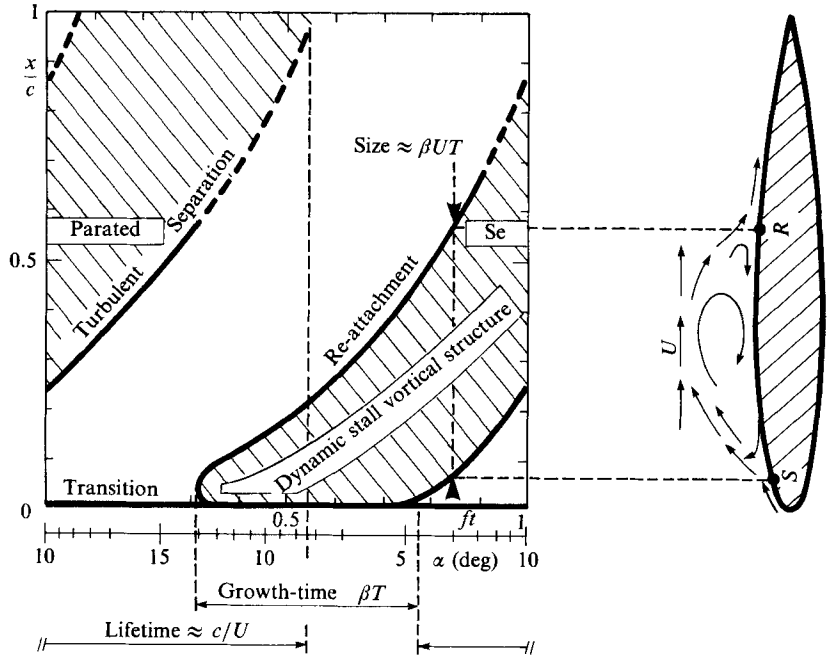

FIGURE 8. Illustration of dynamic stall on space–time diagram for $\bar{\alpha} = 10°$; $\Delta\alpha = \pm 5°$; $U = 3$ m/s; $Re = 3 \times 10^5$; $f^* = 0.65$, under non-cavitating conditions.

represents, in the non-cavitating case $\bar{\alpha} = 0°$, $\Delta\alpha = 5°$, the time at which different phenomena, such as turbulence appearance or disappearance and laminar separation disappearance, occur according to the reduced frequency. It appears that a given phenomenon is more and more delayed when the oscillation becomes faster. In addition, we notice that the unsteady flow rapidly deviates from the quasi-steady flow as the slopes of the different curves are far from zero at the origin $f^* = 0$. Finally, figure 10 shows that the delay effect on the leading-edge cavity birth increases when cavitation becomes more developed at constant oscillation frequency, more especially as the reduced frequency is high. That effect seems to result from the inertial terms $\partial u/\partial t$ whose value and extent increase with the frequency and the development of cavitation.

As a first approximation, convection and delay effects allow us to deduce qualitatively the space–time diagram corresponding to a given oscillation frequency from the space–time diagram corresponding to the quasi-steady case $f^* = 0$. Due to convection, the limits of turbulent, turbulent separated and leading-edge cavity domains have to be scaled according to the $1/f^*$ law, at least in the domain of reduced frequency f^* presently investigated. Secondly, delay shifts the whole diagram by a lapse of time, which is obtained from experimentation, and which gradually increases with reduced frequency.

From the above description, the cavitating flow may appear similar to the non-cavitating one in so far as cavitation roughly fills out the separated domains of the fully wetted flow with vapour and as the convection effect and delay time are of the same order of magnitude for the two cases. However, the two-phase nature of the cavitating flow brings its own unsteady effects, particularly because of the capability of the vapour phase to collapse or explode violently. Those effects are seriously

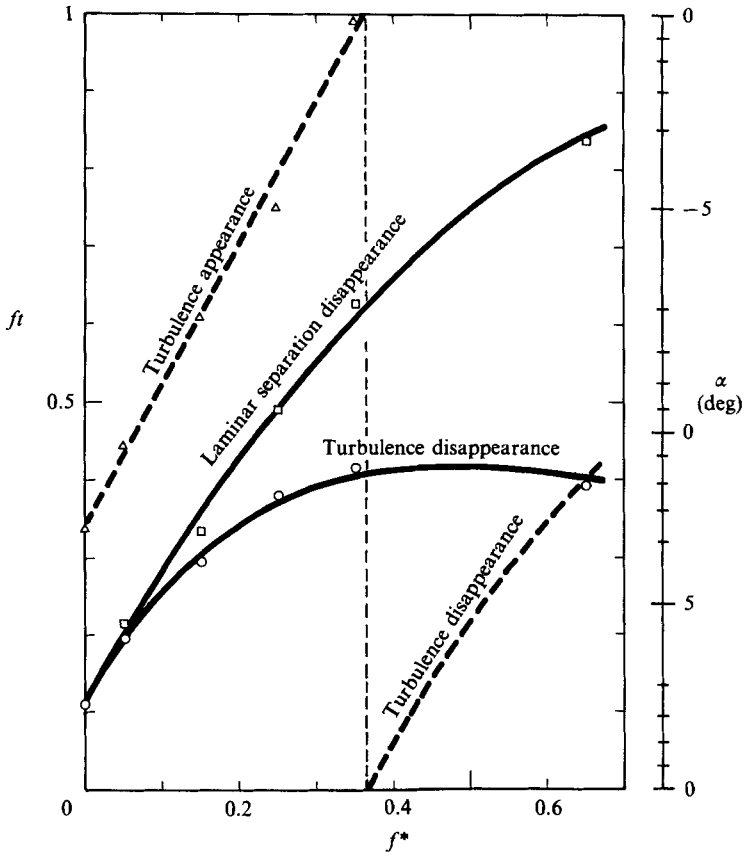

FIGURE 9. Influence of reduced frequency on times at which different phenomena occur during oscillation under non-cavitating conditions for $\bar{\alpha} = 0$; $\Delta\alpha = \pm 5°$; $U = 3$ m/s; $Re = 3 \times 10^5$.

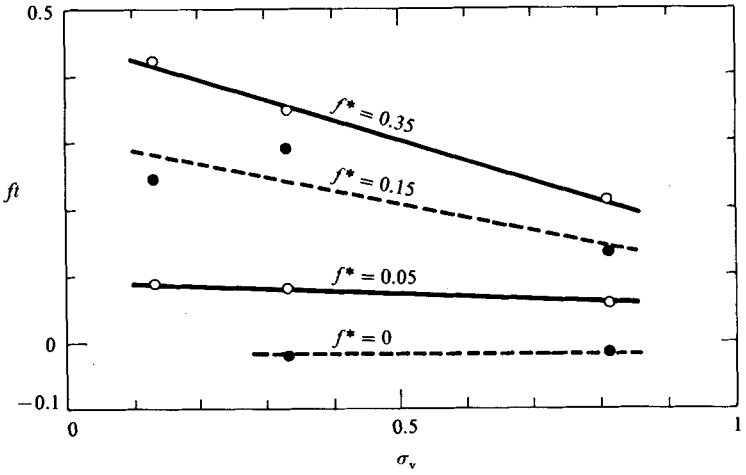

FIGURE 10. Delay effect on the birth of leading-edge cavity on the oscillating hydrofoil for $\bar{\alpha} = 5°$; $\Delta\alpha = \pm 5°$; $U = 6$ m/s; $Re = 6 \times 10^5$.

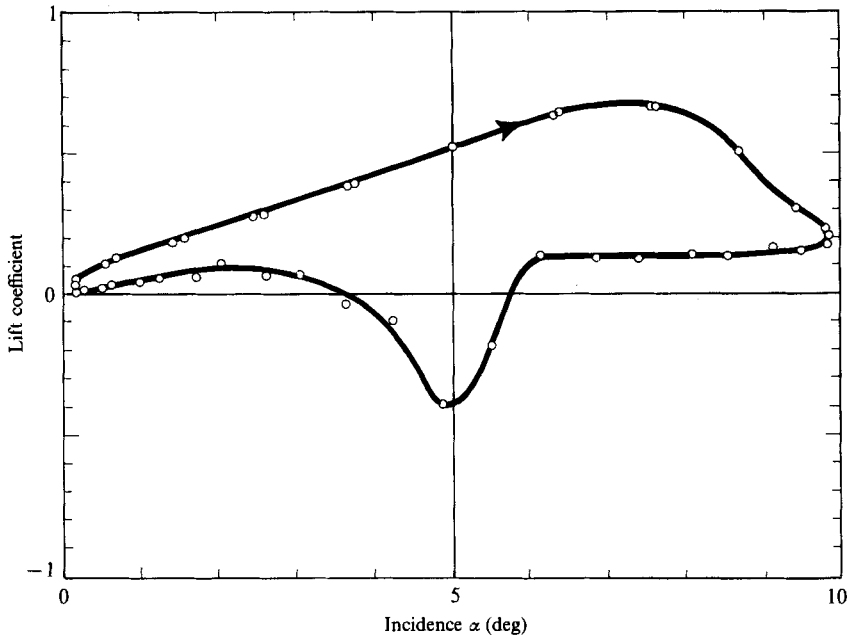

FIGURE 11. Influence of cavity collapse on lift coefficient of the oscillating hydrofoil versus incidence for $\bar{\alpha} = 5°$; $\Delta\alpha = \pm 5°$; $\sigma_v = 0.3$; $U = 7$ m/s; $f^* = 0.05$.

amplified by the general unsteadiness of the flow due to the moving solid boundaries. For example, under some particular conditions of oscillation such as $\bar{\alpha} = 5°$, $\sigma_v \approx 0.4$, the partial leading-edge cavity collapses in a time less than 0.2×10^{-3} s, after it is released in the flow over the foil upper side. The collapse induces a large impulse on forces as shown in figure 11 for the lift coefficient. The negative bump which is grafted on the lift loop corresponds to a lift coefficient variation of about 0.5. Actually, the dynamometer rise time is far larger than the collapse time and the variation of the lift coefficient is larger than 0.5. Likewise, the bump width is overestimated because the measurement results from averaging over several tenths of periods and the instant of the collapse is not fixed inside each period. As a matter of fact, the collapse of the partial leading-edge cavity produces concentrated high pressures which result in a serious pitting of the stainless steel foil surface, whereas the free-stream velocity never exceeded 10 m/s which is far too low to produce any cavitation erosion on stainless steel under steady conditions. This observation confirms previous results obtained by Kruppa & Sasse (1982) who showed that the erosion rate is strongly dependent upon reduced frequency and reaches a maximum for values of reduced frequency between 0.15 and 0.2. So, from an erosion viewpoint, an unsteady flow may be much more aggressive than a steady flow, at equal free-stream velocities.

5. Detachment criterion

One of the major conclusions which result from the present investigation is relative to the interaction between the unsteady boundary layer and the unsteady cavity. Observations and visualizations which have been presented above substantiate the idea that the strong interaction between the boundary layer and the cavity, which

was already pointed out under steady conditions, still plays a prominent role under unsteady conditions. The observed similarities in the behaviour of laminar separation and cavity detachment on the oscillating hydrofoil, together with the negative effect of turbulence on an attached cavity, lead us to generalize the detachment criterion previously proposed for steady cavitating flows to the case of unsteady cavitating flows within the context of the experimental results reported here. The two following points which characterize the interaction between an attached cavity and the boundary layer under steady conditions appear to be still valid under present unsteady conditions:

(i) when a cavity detaches from a solid wall, the boundary-layer flow on the wetted part of the wall, upstream of cavity detachment, is laminar and separates from the wall just in front of the cavity detachment point; in the case of unsteady flows, this does not exclude the simultaneous existence of a limited turbulent zone upstream of cavity detachment;

(ii) if the boundary layer undergoes a transition to turbulence, any attached cavity is swept away as soon as cavity detachment is reached by the turbulent front.

In §2, several timescales were considered. Three among them – namely $1/f$, c/U and l/U – are connected to the global flow configuration. They are larger than the characteristic turbulence time δ/u' by at least one order of magnitude. That point allows us to sketch some features of the flow. The pressure gradient is chiefly determined by the large timescales and lengthscales of the flow. The local interaction between the laminar separation and the cavity detachment is able to fit in a very short time on the continual modifications of the pressure gradient. Besides, if the cavity exists, the detachment position contributes to fix the pressure gradient. Reciprocally, the role of the longitudinal pressure gradient along the foil wall is two-fold, as in the case of the steady flow. Firstly, together with other factors such as external turbulence, it controls the development of the boundary layer until transition to turbulence or laminar separation occurs. Secondly, if laminar separation is present, the cumulative pressure differences from the reference point must also result in the vapour pressure at the detachment point. The detachment criterion then expresses the requirements on the pressure gradient which are imposed by the boundary layer and the attached cavity in order to be compatible.

6. Conclusion

Considering previous experiments under steady conditions and present experiments under unsteady conditions, it appears that the detachment of a cavity is directly connected with the viscous flow.

Under steady conditions, it was proved that a cavity detaches behind a laminar separation of the boundary layer and that an attached cavity is actually not compatible with a turbulent boundary layer.

Unsteadiness affects both the cavity and the boundary layer, essentially through a convection effect and a delay effect. The former causes any phenomenon (transition to turbulence for instance) which initially appears near the leading edge to be convected downstream. The latter brings a delay which increases with unsteadiness to the occurrence of any phenomenon (including cavitation). Notwithstanding those unsteady effects, cavity detachment and laminar separation remain coupled and transition to turbulence still has a negative effect on an attached cavity.

The existence of a region of dead water on a wall is determinant of the existence

of a vapour cavity attached to the wall. A region of still flow is the only opportunity for a cavity to stand in mechanical equilibrium. If not, the cavity behaves like an obstacle to the flow which applies to it a drag force and sweeps it down. Whether the flow is steady or not, separation of the boundary layer is the basic mechanism which generates a dead water zone.

In the case of slender bodies at low angles of attack the boundary layer undergoes a laminar separation at the back of the foil, behind which a cavity is screened from the free stream. If the boundary-layer transitions to turbulent upstream separation, the turbulent flow which is capable of overcoming much larger adverse pressure gradients than the laminar flow will not separate except in the very vicinity of the trailing edge and so the cavity will be swept away. In the case of high angles of attack the flow generally separates from the leading edge under the form of a laminar separation bubble and a vapour cavity grows in the separated zone.

The conclusions presented here have been established in the case of very low nucleus content. Cavitation nuclei are sensible to the region of pressure lower than vapour pressure which exists upstream of the cavity and which is due to the adverse pressure gradient required for separation. According to their critical pressure, this low pressure zone may destabilize cavitation nuclei. Visualizations carried out by Gates & Acosta (1978) have shown that free-stream bubbles may eliminate laminar separation causing a band-type cavitation to be replaced by a travelling-bubble-type cavitation. They point out that the excitation of free-stream bubbles has an indirect effect on cavitation; the primary effect is on the viscous flow past the test body. The present investigation for which disturbances do not come from nucleus expansion but from unsteadiness tend however to confirm this point.

In conclusion, it is to be expected that an attached cavity is basically controlled by the boundary layer, disregarding unsteadiness and nuclei which affect cavitation only via the viscous flow.

Note. A 10 mm film which presents the most typical visualizations of non-cavitating and cavitating unsteady flows around the oscillating hydrofoil (in particular a visualization of cavitating dynamic stall) is available as a loan on request.

This research was supported by the French 'Direction des Recherches, Etudes et Techniques' (Contract DRET 81- 513).

REFERENCES

ALEXANDER, A. J. 1968 An investigation of the relationship between flow separation and cavitation. *N.P.L. Rep. November.*

ARAKERI, V. H. & ACOSTA, A. J. 1973 Viscous effects in the inception of cavitation on axisymmetric bodies. *Trans. ASME* I: *J. Fluids Engng* **95**, 519–527.

BARK, G. & VAN BERLEKOM, W. B. 1978 Experimental investigations of cavitation dynamics and cavitation noise. In *Proc. 12th Symp. on Naval Hydrodyn. Washington DC, June 5–9*, pp. 470–493. Natl Acad. Sciences.

BASU, B. C. & HANCOCK, G. J. 1978 The unsteady motion of a two-dimensional aerofoil incompressible inviscid flow. *J. Fluid Mech.* **87**, 159–178.

BENJAMIN, T. B. 1964 Note on the interpretation of two-dimensional theories of growing cavities. *J. Fluid Mech.* **19**, 137–144.

FRANC, J. P. 1986 Etude physique d'écoulements cavitants. Thesis, Grenoble, France.

FRANC, J. P. & MICHEL, J. M. 1985 Attached cavitation and the boundary layer: experimental investigation and numerical treatment. *J. Fluid Mech.* **154**, 63–90.

GATES, E. M. & ACOSTA, A. J. 1978 Some effects of several freestream factors on cavitation inception of axisymmetric bodies. In *Proc. 12th Symp. on Naval Hydrodyn. Washington DC, June 5–9*, pp. 86–110. Natl Acad. Sciences.

GIESING, J. P. 1968 Non-linear two-dimensional unsteady potential flow with lift. *J. Aircraft* **5**, 135–143.

KRUPPA, C. F. L. & SASSE, G. R. 1982 Cavitation erosion tests with oscillating foil section. In *Proc. 14th Symp. on Naval Hydrodyn. Washington DC, August 23–27.*

MCALISTER, K. W. & CARR, L. W. 1979 Water tunnel visualizations of dynamic stall. *Trans. ASME* I: *J. Fluids Engng*, **101**, 376–380.

MCCROSKEY, W. J. 1982 Unsteady airfoils. *Ann. Rev. Fluid Mech.* **14**, 285–311.

ROWE, A. & KUENY, J. L. 1980 Supercavitating hydrofoils with wetted upper sides. *J. Méc.* **19**, 249–294.

SCHLICHTING, H. 1959 *Boundary Layer Theory.* 4th edn. McGraw-Hill.

SHEN, Y. T. & GOWING, S. 1986 Pressure measurements on an oscillating foil in fully wetted and cavitating conditions. In *Proc. Intl Symp. on Cavitation, April 1986, Sendai, Japan* (ed. H. Murai), pp. 95–102.

SHEN, Y. T. & PETERSON, F. B. 1978 Unsteady cavitation on an oscillating hydrofoil. In *Proc. 12th Symp. on Naval Hydrodyn. Washington DC, June 5–9.* Natl Acad. Sciences.

SHEN, Y. T. & PETERSON, F. B. 1980 The influence of hydrofoil oscillation on boundary layer transition and cavitation noise. In *Proc. 13th Symp. on Naval Hydrodyn. Tokyo, October 6–10,* pp. 221–241. Natl Acad. Sciences.

VAN DER MEULEN, J. H. J. 1980 Boundary layer and cavitation studies of NACA 16-012 and NACA 4412 hydrofoils. In *Proc. 13th Symp. on Naval Hydrodyn. Tokyo*, pp. 195–219. Natl Acad. Sciences.

WOODS, L. C. 1964 On the theory of growing cavities behind hydrofoils. *J. Fluid Mech.* **19**, 124–136.